Fuel 362 (2024) 130851

Contents lists available at ScienceDirect

Fuel

journal homepage: www.elsevier.com/locate/fuel

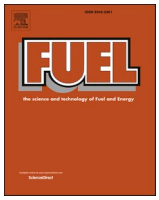

Full Length Article

Experimental characterization of direct injection liquid ammonia sprays under non-reacting diesel-like conditions

Raul Payri, José M. García-Oliver, Gabriela Bracho, Jiawei Cao *

Departamento de Clean Mobility & Thermofluids, Universitat Politécnica de València, Camino de Vera s/n, 46022 Valencia, Spain

ARTICLE INFO

Keywords:
Ammonia
Direct injection
Liquid length
Tip penetration
1D model

ABSTRACT

Ammonia is seen as a promising fuel to replace fossil fuels internal combustion engines, given the advantages of zero carbon emission and extensive experience in its synthesis at large scale. The ignition of ammonia in direct injection engine is still a challenge due to its unfavorable combustion characteristics, but the investigation of ammonia spray characteristics is an important step to shed light on the optimum combustion strategy. In this paper, the evolution of direct injection ammonia sprays was measured at engine-like conditions generated in a constant pressure facility by means of diffused back-illumination imaging and schlieren. In a first step, ammonia spray behavior is compared against that of Diesel fuel. Experimental results show a slower penetration of ammonia mainly due to a lagging starting penetration phase, which cannot be later recovered. In terms of liquid length, initial stages show the same pattern as for ammonia, while a shorter stabilized liquid length can be observed. Parametric trends over different operating conditions show a similar behavior to Diesel against ambient density and temperature, as well as with injection pressure and nozzle diameter. Such results, backed up by the application of a 1D spray model developed for Diesel-like fuels, suggest that ammonia sprays under non-reacting conditions have a mixing-controlled evolution.

1. Introduction

Current propulsion systems for heavy duty vehicles such as trucks and ships are based on combustion engines powered by fossil fuels due to their high thermal efficiency and reliability, but producing big amounts of harmful substances such as NO_x and particulate matter, which are dangerous to the environment and the human health. On a more global level, the transport and industrial sectors contribute to greenhouse gas (GHG) emissions [1], especially with the production of carbon dioxide (CO_2). Since the Paris Agreement in 2016, international organizations are taking actions to mitigate the global warming and to achieve the carbon neutrality in the energy and transport sectors [2]. One of the measures in combustion engines is to replace the traditional fossil fuels by carbon-free or carbon–neutral fuels. One of the favorite candidates is hydrogen because of the absence of carbon atoms, and hence of CO_2 in the combustion products. However, certain undesirable properties of hydrogen, such as its low density and high flammability range, are a challenge for its secure storage and transportation [3].

Another carbon-free fuel that is gaining attention recently is ammonia (NH_3), since the technology available for its production and the storing infrastructure are more mature than for hydrogen [4]. It has also a higher volumetric energy density and can be easily liquified at room temperature under 9 bar (at these conditions energy per unit volume in liquified ammonia is about 1.6 times higher than that of liquified hydrogen) [5]. Moreover, ammonia could be considered as a sustainable fuel, if obtained using hydrogen produced from renewable sources [6] (i.e., the so-called green hydrogen). Ammonia combustion does not produce CO_2, but the nitrogen element leads to a possibility of increased emission of nitrogen oxides [7]. In [5], Novella et al. performed an evaluation of the environmental impact in road transport, in terms of greenhouse gas emissions, using a virtual model and a Life Cycle Assessment (LCA) of a medium-duty vehicle. They found that ammonia fully produced from renewable resources can decrease the greenhouse gas level up to 43 % compared to Diesel and gasoline with the same technical characteristics. The main contributor for this reduction was the fuel production process (fully renewable). Besides, ammonia has poor combustion characteristics, such as low laminar flame speed, high auto-ignition temperature and narrow flammability range compared to other traditional fuels, which makes its direct application in internal combustion engines more complicated. In addition, if combustion is incomplete, it tends to form highly hazardous

* Corresponding author.
E-mail address: cjjiawei@mot.upv.es (J. Cao).

https://doi.org/10.1016/j.fuel.2023.130851
Received 13 November 2023; Received in revised form 14 December 2023; Accepted 30 December 2023
Available online 8 January 2024

Nomenclature

ASOI	after the start of injection
Ca	area coefficient
Cd	discharge coefficient
CI	compression ignition
CMT	Clean Mobility & Thermofluids
CO_2	carbon dioxide
CPF	constant-pressure flow facility
DBI	diffused back-illumination imaging
D250	nozzle diameter 250 μm
D300	nozzle diameter 300 μm
d0	orifice diameter
ECN	Engine Combustion Network
f	mixture fraction
f_{evap}	evaporation fuel mass fraction at the edge of the liquid spray
GHG	greenhouse gas
IL	intact length
LL	liquid length
LL*	constant coefficient of liquid length scaling
L-V	liquid–vapor
k	coefficient in vapor penetration correlation
NO_X	nitrogen oxides
ROI	rate of injection
S	vapor tip penetration
SI	spark ignition
t	time
$\dot{M}_0$	momentum flux
ρ_f	fuel density
ρ_a	ambient density
u_0	velocity at the orifice outlet
θ	spray angle
θ_1	spray angle at near field
θ_2	spray angle at far field
1D	one-dimensional

compounds such as NO, NO_2 and N_2O [8]. To overcome these unfavorable characteristics, numerous investigations have been carried out recently under different combustion strategies.

Both spark ignition (SI) and compression ignition (CI) engines have been studied and adapted to run with ammonia. In SI engines, some works have blended ammonia with other fuels with higher reactivity, like hydrogen, methane or gasoline [9–11]. Also, SI engines fueled with pure ammonia have been demonstrated to achieve high thermal efficiency when the combustion chamber is modified and the compression ratio is increased, similar to those geometries and values used in CI systems [47], [12,13]. However, the emissions levels of NO_x and unburned fuel are considerably high due to wall quenching effects and fuel that remains in the crevice region.

Regarding CI engines, the dual-fuel combustion approach is preferred due to the high auto-ignition temperatures required by ammonia. Previous works have proposed the use of dual-fuel configuration with air-ammonia homogeneous mixture and a small pilot of a low carbon-based fuels or with conventional Diesel [14–16]. Their studies showed that the concept was feasible, with acceptable efficiencies, however they suffered from high NO_x emissions and unburned ammonia due to large quenching effects and residuals of the fuel in the crevice region.

Other works proposed to inject ammonia directly into the cylinder close to the TDC to avoid fuel slip due to near-wall quenching, still using a more reactive fuel as pilot (Diesel, OMEx) ignition source [8]. In this situation, ammonia would burn mainly in a diffusive manner if the pilot were injected immediately or could burn in a partially premixed manner if the pilot injection is delayed. The diffusive combustion of ammonia might lead to lower NO_x emissions when compared to premixed case [8,17,18].

Finally, the work in [19] presented a numerical study of a method that enabled the combustion of direct pure ammonia injection (with no pilot assistance) in a two-stroke low-speed marine engine thanks to the high in-cylinder temperatures achieved in their system. The approach is named high-temperature cylinder gas recirculation, where high-temperature gas is recirculated to the cylinder at a fixed angle before the injection time increasing the temperature up to 1200 K and the swirl ratio in the cylinder. Results show that the increase of cylinder temperature promotes ammonia ignition and increases thermal efficiency to 50 %.

From the aforementioned literature, ammonia combustion is sensitive to the spray characteristics, influencing the engine performance [17,19]. To understand the spray development, it is essential to have access to experimental data in the required operating conditions that shed light on the behavior of the liquid when it is delivered into the combustion chamber, how it atomizes, mixes with the surrounding air and the way it evaporates. In this regard, extensive information is available for conventional fuels (such as Diesel or biofuel), while analysis of ammonia sprays under direct-injection high-pressure conditions are scarce. In general, the number of investigations on the spray characteristics of ammonia is small and mainly concerned with the conditions at room temperature or low pressure injection levels. For example, spray tip penetration and fuel concentration were measured in [20] for an ammonia jet with the variation of both injection and ambient pressure at room temperature. They found that ammonia has a similar tip penetration and jet angles as methane, but the equivalence ratio is much smaller. More recently, the mixture formation of sprays under direct-injection conditions was characterized in [17] by means of optical techniques in a rapid-compression-expansion machine. Shadowgraphy and Mie-scattering measurements were used in non-reacting conditions to validate a spray 1D model. The maximum injection pressure measured was 560 bar using two nozzle diameter values of 940 μm and 980 μm. The experimental and numerical results of one operating condition of direct-injection at 600 bar in [21] analyzed the vapor-phase and liquid-phase penetration evolution of the spray, and concluded that for that operating condition the break-up and evaporation models (KH-RT and Frossling respectively), extensively used for Diesel sprays, can be also used for predicting ammonia injection behavior.

Within this context, the present study aims to describe the liquid- and vapor-phase evolution of ammonia sprays at CI engine conditions with high injection pressure levels, namely up to 800 bar. For this purpose, optical experiments are performed in a high-pressure high-temperature vessel. Liquid length is quantified by means of the diffused back illumination (DBI) technique, and vapor spray penetration is determined using the Schlieren method. The main contributions of this work are indicated as follows:

- Description of the injection system and the methodology employed for delivering liquid ammonia into the combustion chamber, minimizing the phase change in the supply system as well as the injector body, even at high injection pressure.
- Production of a highly relevant experimental dataset of liquid and vapor spray, for a wide parametric matrix in terms of chamber gas temperature (from 700 up to 900 K), gas density (22,8 and 30 kg/m^3), injection pressure (from 400 up to 800 bar) and two nozzle diameters (250–300 μm).

- Analysis of ammonia sprays using a well-established 1D spray model, which has been previously developed for Diesel-like sprays.

The article is structured as follows. Section 2 describes the methodology, including test facility, fuel injection system, optical techniques and processing routines. Then, Section 3 presents the results, starting with a comparison between ammonia and a conventional fuel, highlighting the main differences between fuels. Then the effect of the studied parameters on the liquid phase and the vapor phase are shown. The last section describes the 1D model adaptation to the new fuel scenario followed by the main conclusions of the work.

2. Experimental methodology and image processing

In this section, the introduction of the test facility and the injection system for liquid ammonia is first presented, then the fuel properties of ammonia and Diesel and investigated condition are discussed. Finally, the optical techniques adopted in this paper are described, and the specifications are also provided.

2.1. Test facility and fuel injection system

The facility utilized for the experimental campaign is a high pressure and high temperature test rig that can generate a thermodynamic atmosphere with temperature up to 1100 K and pressure up to 15 MPa. The thermal condition in the rig is achieved through a continuous gas flow at a speed lower than 0.3 m/s, hence the atmosphere inside the rig can be considered as quiescent. The rig is classified as a constant-pressure flow (CPF) facility and has an effective volume of 15 L, allowing for the investigation of free spray penetration. Three out of the four sides of the rig are equipped with two pairs of windows, each with a diameter of 128 mm and 181 mm, distributed in a cross pattern.

Apart from the vessel, the other sections can be mainly described as the gas circuit system, heating system and control system. The air compressor supplies high-pressure air to operate it as an open circuit or combine it with nitrogen as a closed circuit. This enables the simulation of the degree of exhaust gas recirculation by reducing the oxygen concentration in the charge mixture, or even with full nitrogen (non-reacting condition in this paper). The dry gas then enters the chamber through a 30-kW electric heating system. The valve at the bottom of the chamber is used to adjust the gas flow rate to control and maintain the temperature and pressure inside the chamber. To monitor the thermal state inside the chamber, a pressure sensor is placed at the chamber inlet, and three temperature sensors are installed near the injector. The facility has been extensively used to produce a large amount of measurements on the spray and combustion process, more information about the facility can be found in [22–24].

A Bosch solenoid injection system with a convergent single hole nozzle has been employed for ammonia direct injection. Liquid ammonia is extracted from a high-pressure container, then it is cooled down in the pipe to prevent cavitation and fed into a high-pressure pneumatic pump. To guarantee that the ammonia remains in liquid phase inside the injector body, two solutions have been implemented:

(1). The pressure of the return-leakage line is increased up to 10 bar, using a dedicated back pressure valve and a tank.
(2). The injector holder is designed with a cooling system with glycol that is circulated at a minimum possible temperature of 15 °C. All the return lines of the system are collected and directed towards an acid trap, formed by a large water container, similar to the one employed in [19].

With the described configuration, the system could be operated under stabilized conditions up to an injection pressure of 800 bar. For each operating condition, 20 injection events were recorded with the frequency of 10 s between two successive events to ensure the constant thermodynamic environment for each injection event. The injector energizing time was set at 2000 μs for all conditions.

Injections fueled with Diesel are performed for comparisons. The properties of both fuels are given in Table 1. The multi components in diesel correspond to a range of boiling point rather than one value for ammonia. The experimental conditions are summarized in Table 2, including the effects of ambient temperature, ambient density, nozzle diameter and injection pressure. The reference condition for the present study is denoted in bold character, and the comparison between fuels is also performed at this condition. Note that D250 is the abbreviation of nozzle with the diameter at 250 μm, and D300 means the nozzle diameter at 300 μm (see Fig. 1).

2.2. Optical techniques

2.2.1. Diffused back-illumination imaging

In the present study, diffused back-illumination imaging (DBI) is used to measure the amount of light attenuated by liquid droplets, which is the recommended diagnostics for measuring the spray liquid length within Engine Combustion Network [26]. In the past, it has been adopted for the liquid length measurement of many kinds of fuels [27,28]. Fig. 2.a presents the schematic of optical setup. On the left side, a high-power red LED provides the light source, and the generated light beam goes through a diffuser. On the right side, a spherical lens with a focal length of 450 mm placed outside the window collects the light beam and directs it into the high-speed CMOS camera placed at the focal length plane. The specifications of the setup are given in Table 3.

2.2.2. Single-pass schlieren

The schlieren technique is based on the deviation of a parallel light beam when it passes through a non-homogeneous fluid [29]. Light direction is changed due to the density and hence refracted index gradients along its path, especially when if finds the spray and the hot atmosphere inside the rig. Spray contours can be extracted from the recorded images, and characteristics such as vapor spray penetration and spray angle can be obtained. Fig. 2.b depicts the schematic of the single pass schlieren setup. Similar optics arrangement can be seen in [30]. On the left side, a xenon white lamp served as the light source, with an iris diaphragm of 2 mm diameter placed before it to generate a point incident light. This setup was positioned at the focal length plane of a parabolic mirror, with an incident angle of 20 degree to minimize the effect of beam straightening. The parallel light then entered the chamber, covering the fields where the ejected fuel propagates. On the right side, the same spherical lens used in DBI remains to collect the deviation beam caused by the non-homogeneous spray. A 5-mm iris diaphragm was placed in the focal length of the spherical lens, and a high-speed CMOS camera behind was used to capture the focused light beam. Experiments with DBI and schlieren were not simultaneous, but the images

Table 1
Fuel properties for Diesel and ammonia.

	Diesel [22]	Ammonia [25]
Cetane number [–]	53	–
Lower heat value [MJ/kg]	42.97	18.6
Fuel density [kg/m^3]	834[a]	617.5[b]
Aromatics concent [% (vol.)]	27	–
Kinematic viscosity [mm^2/s]	2.8[c]	14[d]
Initial boiling point [K]	423.98	239
Final boiling point [K]	636.98	239
Flash point [K]	–	405
Enthalpy of vaporization [kJ/mol]	80.2[e]	23.37[f]

[a] Value at 15 °C.
[b] Value at 21.1 °C.
[c] Gaseous state at 40 °C
[d] Value at 300 K.
[e] Value at 298 K and 1 atm.

Table 2
Test conditions. Bold characters are used for the reference conditions.

Parameter	Values
Oxygen concentration [%]	0
Ambient temperature [K]	700, 800, **900**
Ambient density [kg/m^3]	**22.8**, 30.4
Injection pressure [bar]	400(500*), 600, **800**
Nozzle diameter [μm]	250, **300**

* Only for the large nozzle diameter test.

throughout Schlieren share the same image specifications as DBI. The only difference is the shutter speed of schlieren, which is at 0.6 μs.

2.2.3. Image processing

Image processing is carried out using home-made software, with the following steps.

- Background subtraction: the first 15 images acquired before the start of the injection are averaged as a background. The turbulence in the chamber throughout the image recording may cause some noise, but the background can be seen as quasi-steady state during the injection process.
- Contour detection: the approach employed by Siebers [31] was adopted, and the contour was calculated by image binarization. The threshold in the dynamic range was set at 3 % in DBI and 5.5 % in Schlieren.
- Contour analysis: spray liquid length (LL), vapor penetration (S) and spray angle (θ) can be obtained after the contour detection (Fig. 3). For DBI images, the threshold for the image binarization helps to mitigate the noise effects and ensure a robust detection of the liquid phase silhouette, and the liquid length was obtained from the light extinction profile on the axis of centreline downstream of the nozzle outlet, which has been discussed in [28]. Vapor penetration is defined as the longest distance of the contours in the downstream of the nozzle outlet, and spray angle was based on the segment insides the contour that coincides with distances of 12 % and 60 % of the instantaneous vapor penetration [32].

3. Results and discussion

In this section, the comparison of ammonia and Diesel will be presented firstly in terms of the spray images, spray penetration and spray angle obtained from DBI and schlieren, then the effect of parametric variation at engine-like conditions on the liquid length and vapor penetration is analyzed. Finally, the validation of 1D model is presented.

3.1. Transient spray evolution of Diesel and ammonia at reference condition

Fig. 4 shows a series of representative spray images throughout DBI and Schlieren for Diesel and ammonia at the reference condition. On global terms, the ammonia jet exhibits a similar cone-like shape compared to a Diesel one, the main differences being a narrower spray angle and a lighter appearance of the images in liquid phase. The evolution shows that vapor tip penetration steadily increases with time, while the liquid one reaches the well-known maximum liquid length. To further quantify these trends, the temporal evolution of the sample-averaged liquid and vapor penetrations for both fuels are presented in

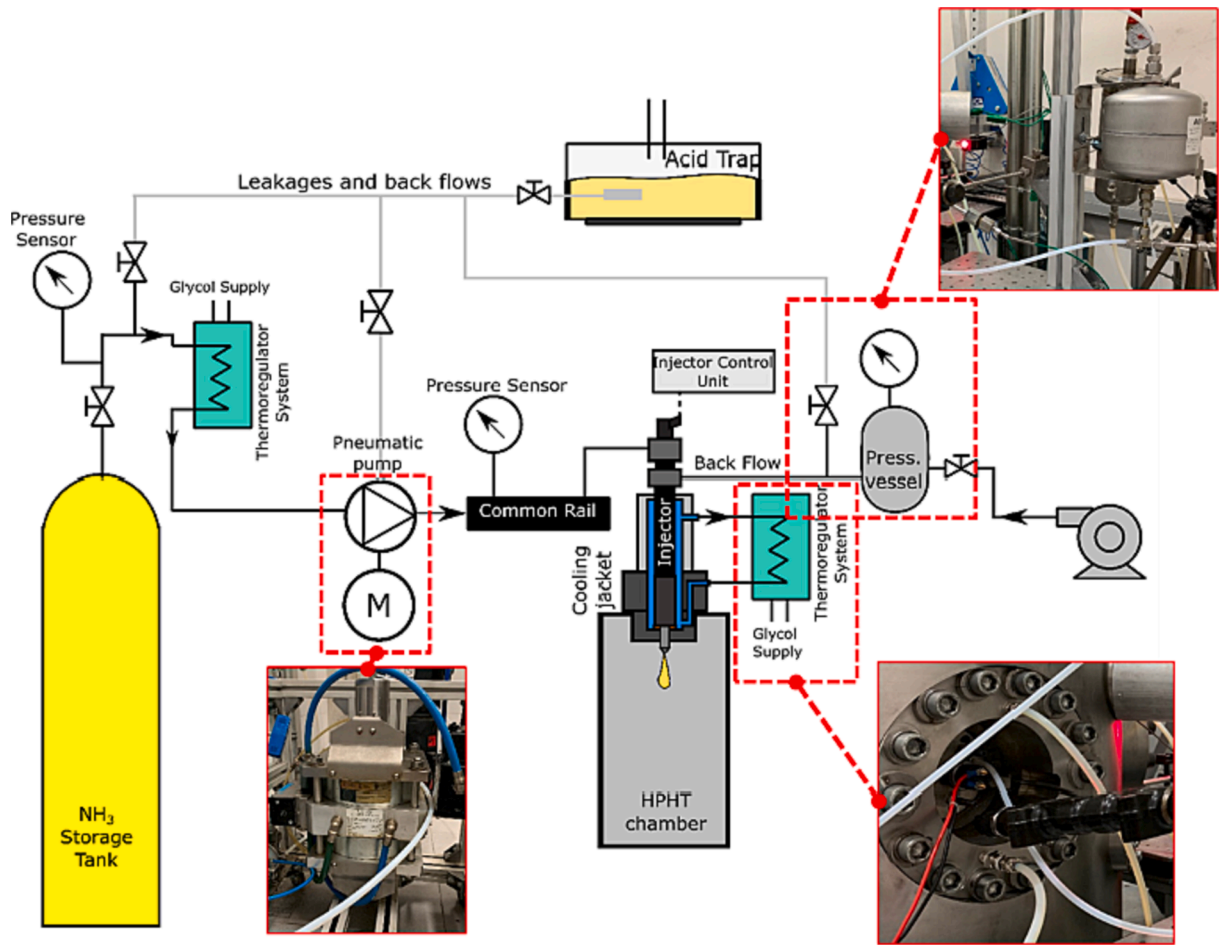

Fig. 1. The schematic of ammonia direct-injection system.

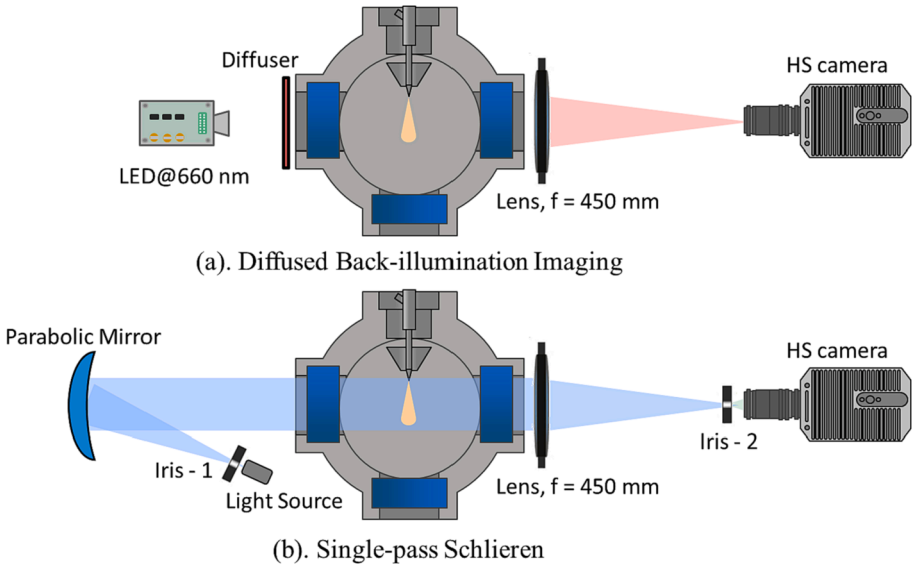

Fig. 2. Optical setup for Diffused Back-illumination Imaging (a) and Single-pass Schlieren (b).

Table 3
Specifications of the optical setup and cameras.

	DBI/Schlieren
Camera	SA-X2
Sensor type	CMOS
Lens diameter	450 mm
LED pulse duration	10 ns / -
Diaphragm gap	- / 5 mm
Frame rate	60 kfps
Resolution	768 × 272
Shutter time	15 / 0.6 μs
Pixel – mm	4.2
Recorded injection cycles	20

Fig. 5, and the evolution of spray angle from schlieren images is shown in Fig. 6. Each curve is an average of 20 cycles, and the uncertainty is plotted as shadow with a lighter color.

In the initial phase, where liquid and vapor penetration overlap, the process can be characterized into two stages according to the penetration slopes: the first stage is from the start of injection until 0.3 ms ASOI for Diesel and until 0.6 ms ASOI for ammonia. A linear trend of penetration with time is observed for both fuels, but a slower penetration rate can be found in ammonia case that hints at a lower momentum of the spray. This can be related to the internal flow and dynamic operation of the injector when ammonia is used, which is affected by a high friction in the sac caused by the high fuel viscosity, and results in a slower needle lift. DBI images confirm that it takes longer for the ammonia case to launch the injection after the start of energizing. From the end of the first stage to the moment when the liquid and vapor phase start to separate, ammonia shows an increase in tip penetration rate, while Diesel exhibits a decrease. For ammonia, this is due to the very slow initial behaviour, that later transitions to a more stabilized evolution when the needle is fully open. Comparing the spray images, ammonia spray profile at 0.8 ms ASOI is similar to Diesel at 0.4 ms ASOI, but the radial expansion is more significant in the steady region, rather than the transient region for Diesel.

After the initial phase, the liquid spray penetration tends to stabilize at a value around 40 mm for ammonia spray and 60 mm for Diesel spray. The time evolution of liquid length in the Diesel case is pretty flat, while ammonia shows some fluctuations. Tip penetration keeps increasing with time, and differences between fuels (essentially a time shift) hint at a very similar penetration rate. Furthermore, spray tip cone angle after

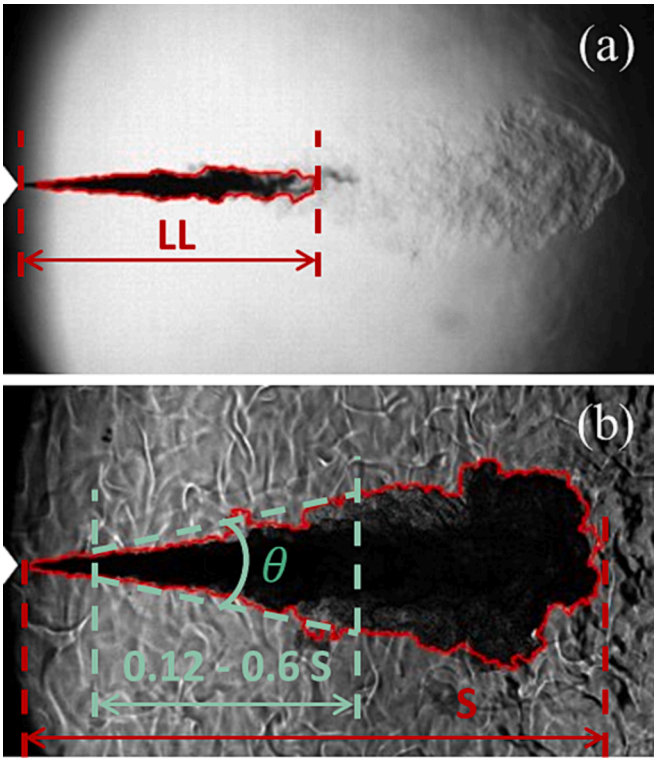

Fig. 3. Example of spray contours through Diffused Back-illumination Imaging (a) and Single-pass Schlieren (b).

1.2 ms ASOI is also similar between ammonia and Diesel. Both effects hint at a quasi-steady penetration period for both ammonia and Diesel. Therefore, the use of ammonia creates differences mainly during the initial stages most probably due to transient needle lift effects. Once injection stabilizes, ammonia spray behaves very much as s Diesel one, i.e., a fully developed turbulent spray.

3.2. *Parametric variations. Liquid length*

Different operating variables are analyzed here. First, the effect of the injection pressure on liquid spray penetration is shown in Fig. 7, and

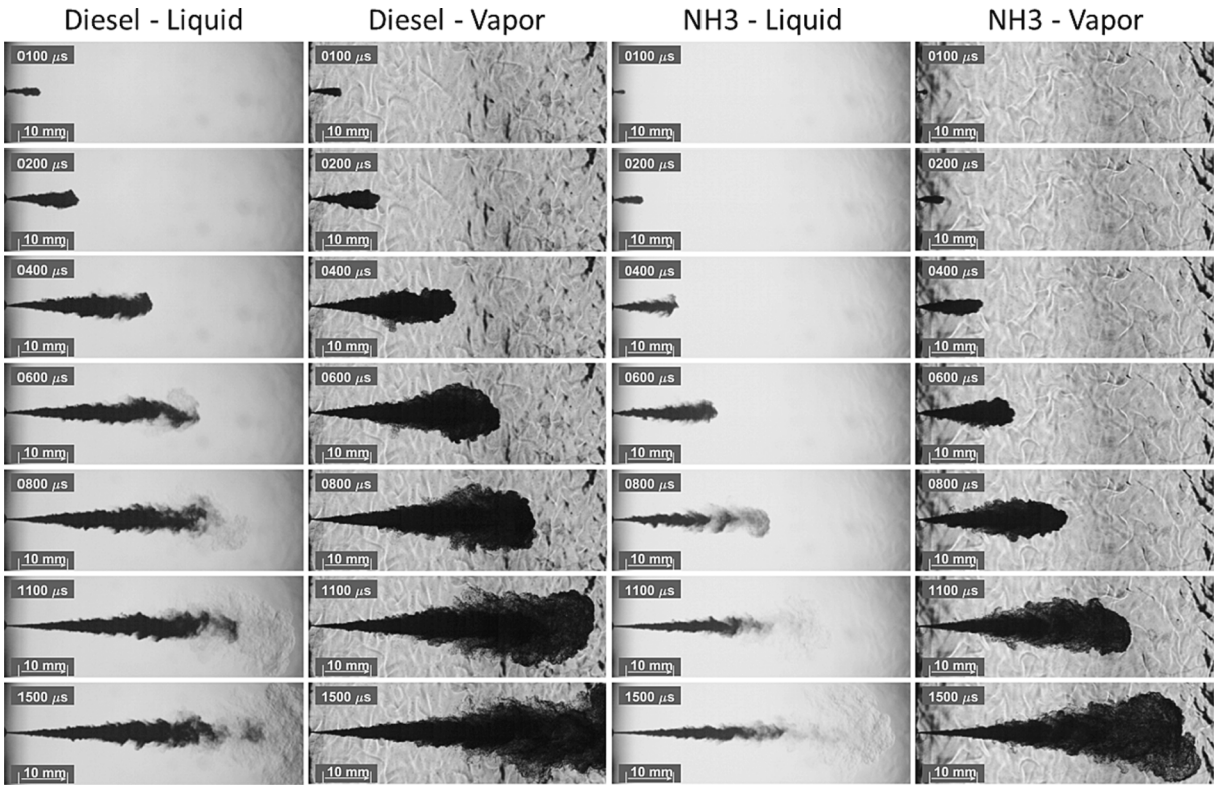

Fig. 4. A time sequence of spray images by DBI and Schlieren. The sequence from top to bottom consists of the transient region (the first to the fourth) and the stabilized liquid length region (1500 μs ASOI). Condition (ρ_a = 22.8 kg/m^3, T_a = 900 K, D_0 = 300 μm, P_r = 800 bar).

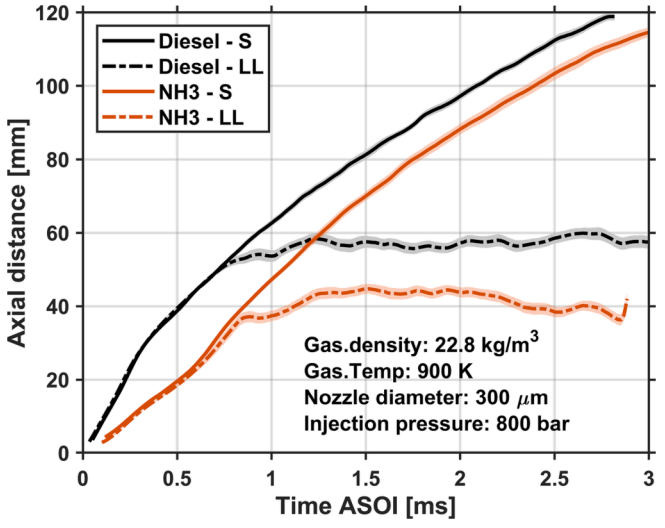

Fig. 5. Vapor and liquid spray penetration evolution for Diesel and ammonia. Condition (ρ_a = 22.8 kg/m^3, T_a = 900 K, D_0 = 300 μm, P_r = 800 bar).

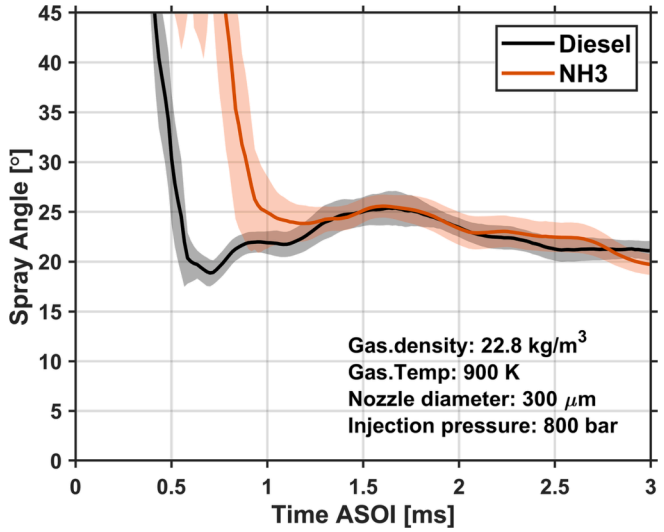

Fig. 6. Spray angle evolution through Schlieren imaging for Diesel and ammonia. Condition (ρ_a = 22.8 kg/m^3, T_a = 900 K, D_0 = 300 μm, P_r = 800 bar).

the comparison between different nozzles is also presented. Under the variation of injection pressure and nozzle diameter, the spray liquid penetration shows a similar evolution where it increases in the initial phase and then stabilizes. At the initial phase, a faster penetration was observed at a higher injection pressure because of high velocity at the orifice outlet and a faster opening of injector nozzle [23]. This behavior is more significant for the larger nozzle because of the larger momentum flux. In the stabilized region (1.5 to 2.5 ms ASOI), liquid penetration is not very sensitive to injection pressure, with only a slight decrease when injection pressure drops to 400 bar. It takes longer for the larger nozzle to reach stabilization, and it exhibits a more significant fluctuation, most probably due to its stronger phase transition in the larger sac. The present trends agree with previously obtained results for Diesel fuel [31].

Fig. 8 presents the liquid spray penetration of ammonia under the variation of ambient temperature and ambient density for D300 at injection pressure 800 bar. The initial linear phase can be seen to have slightly different duration depending on ambient temperature and density, which can be due to slightly different interaction with the slow momentum sprays with the ambient air that are hard to explain based on the available experimental information. After that, the evolution of the

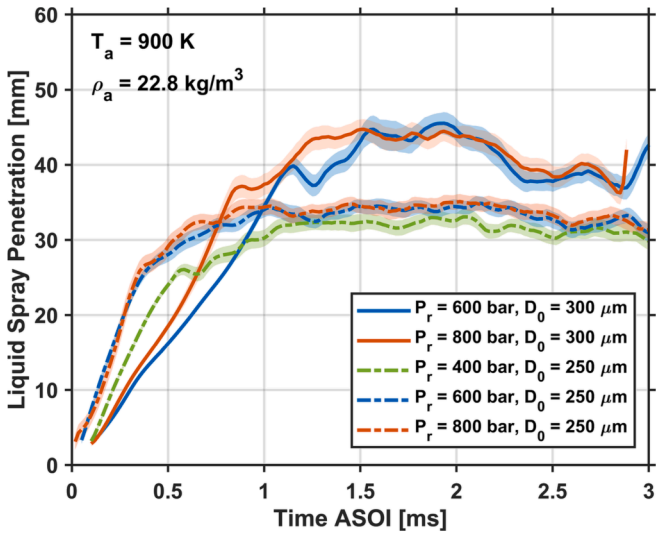

Fig. 7. Time-evolution liquid spray penetration for ammonia with two different nozzles (D_0 = 250 μm, 300 μm) at different injection pressures (P_r = 400, 600, 800 bar). Colour shades present the liquid length variation, and the line type shows the date from different nozzles. Ambient condition (T_a = 900 K, ρ_a = 22.8 kg/m^3).

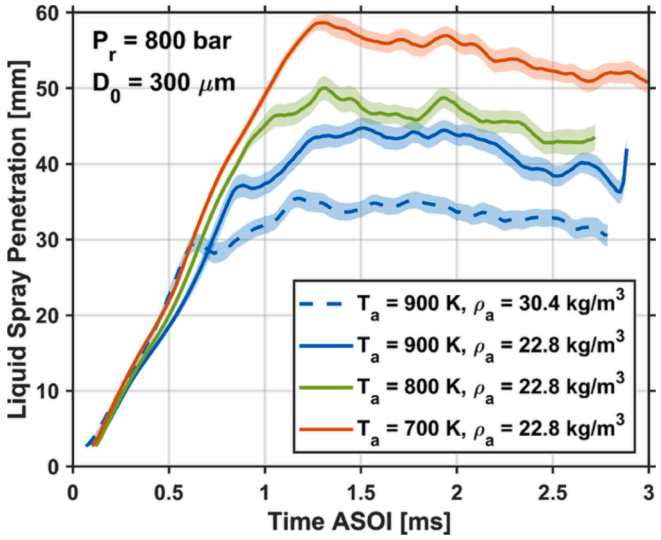

Fig. 8. Temporal liquid spray penetration for ammonia at injection pressure 800 bar for D300 with different thermal atmospheres, including the variation of ambient temperature and density.

transient liquid tip is quite similar, with a very similar penetration rate and just a slight time shift. Eventually, liquid penetration enters the stable region at a distance that depends on ambient temperature and density. Quasi-steady values decrease with an increase in both ambient variables [31].

Fig. 9 (left) shows analysis of the average quasi-steady value of liquid length (*LL*) of ammonia spray together with variations of ambient temperature, density and injection pressure for both nozzle orifices. The values are obtained by averaging the time evolution within the stable region from 1.5 ms ASOI to 2.5 ms ASOI. As expected, longer liquid length was observed at a larger nozzle due to the higher injection rate. A rise in ambient density causes a faster spray breakup and fuel–air mixing rates, and an increase in ambient temperature increases the enthalpy entrainment into the spray both resulting in a shorter liquid length [33]. For the injection pressure between 600 bar and 800 bar, the liquid length is almost constant, while it is slightly shorter at a lower injection pressure. Even though, the discrepancy of liquid length caused by the injection pressure is also within 5 %.

The very small effect of injection pressure on maximum liquid length is a first indicator that the ammonia spray behaves very similar to mixing-controlled Diesel sprays. In this sense, scaling laws based on fuel–air mixing controlled hypotheses are usually adopted to evaluate the liquid length of direct injection sprays [34]. Following this idea, a scaling law can be defined in eq. (1) for *LL* following [24].

$$LL = LL^{*} \cdot \frac{d_0 \cdot \sqrt{\frac{\rho_f}{\rho_a}}}{tan\left(\frac{\theta}{2}\right) \cdot f_{evap}} \tag{1}$$

where LL^{*} is a constant coefficient, θ is spray angle, f_{evap} is the evaporation fuel-mass fraction for the given mixture, d_0 is the orifice diameter, ρ_f is the fuel density and ρ_a is the ambient density. The equation above indicates that the liquid length will be linearly dependent on the orifice diameter and the square root of the ratio of fuel to air density, and inversely dependent on the evaporation mixture fraction and spray angle. In other words, LL^{*} would be the same across the conditions. Fig. 9 (right) presents the calculated LL^{*} (Liquid length* [–] in Y label), with a constant spray angle equal to 22.5°. The latter parameter was not obtained from schlieren measurements due to the well-known uncertainties involved in accurately measuring spray angle by means of schlieren [35]. Including all the conditions, the averaged LL^{*} is 1.798 with the uncertainty of 6.3 %, which can be acceptable as the uncertainty of measurement. Most noticeable deviations occur at some conditions with the lower injection pressure, where injection operation was more unstable.

3.3. Parametric variations. Vapor spray penetration

As discussed before, tip penetration for ammonia sprays has a very similar evolution after the initial transient phase, and the scaling of the liquid length can be formulated from a mixing-controlled point of view. Following this reasoning path, a scaling law for tip penetration can be formulated for ammonia sprays similarly to Diesel ones that will help analyze parametric variations. In particular, extensive research in the literature shows that vapor tip spray penetration is mainly dependent on ambient density, orifice diameter, injection velocity and spray angle [36,37]. In particular, it was shown in [38] that for a top hat injection rate profile, Diesel-like sprays follow a square-root of time evolution as shown in Eq. (2) with similar parameters as for the liquid length (Eq. (1)) plus the nozzle momentum flux $\dot{M}_0$ and injection velocity u_0.

$$S(t) = k\left(\dot{M}_0/\rho_a\right)^{0.25} (t/\tan(\theta/2))^{0.5} \propto \left(\frac{u_0 d_0}{\tan(\theta/2)} \sqrt{\frac{\rho_f}{\rho_a}} t\right)^{0.5} \tag{2}$$

Fig. 10 (left) shows the effect of nozzle diameter on the vapor penetration of ammonia inert spray at the reference condition, i.e., ambient temperature at 900 K, ambient density at 22.8 kg/m^3, and injection pressure at 800 bar. The liquid penetration was also added as a reference. Initial penetration is mainly controlled by the needle lift, and a faster ramp up at D250 causes an initial faster penetration. However, after this initial injection period, a faster penetration rate is observed at D300, which eventually offsets the slower initial period and catches up with the D250 case at 2 ms. Fig. 10 (right) shows the evolution of the tip penetration rate (dS/dt). To eliminate the time lag effect of ramp up, penetration rate is presented against tip penetration, with a decay that mimics a dS/dt ~ 1/S evolution, which can be justified from Eq (2). The larger nozzle shows a faster penetration at every axial position by a factor that is very similar to the square root of the nozzle diameter ration ($\sqrt{300/250}$ = 1.09), consistently with the scaling law in Eq. (2).

Fig. 11 shows a sample of the comparison of vapor spray penetration under different ambient temperatures. Ambient density is set at 22.8 kg/

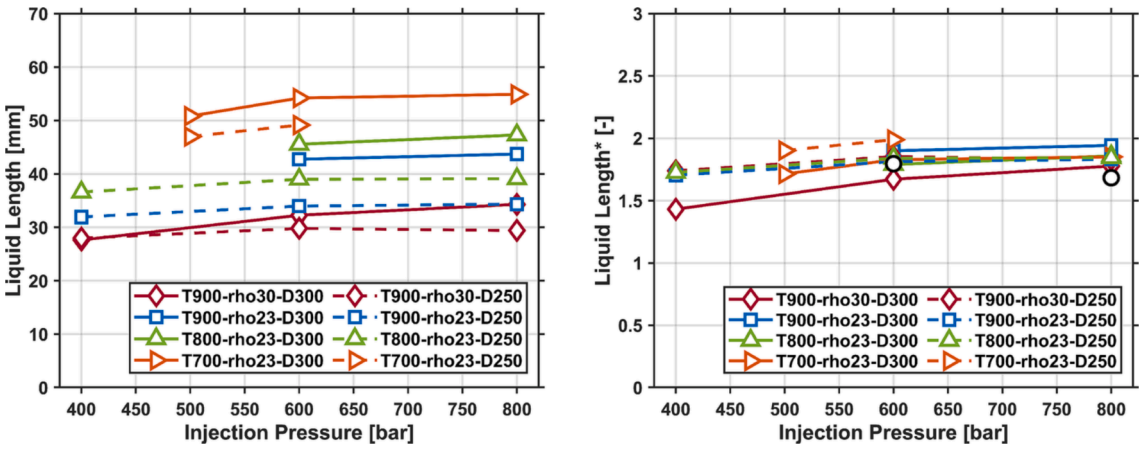

Fig. 9. Liquid length (left) and Liquid length* (right) dependence of injection pressure at the variation of ambient temperature and density. Solid: $D_0 = 300\,\mu m$; Dash: $D_0 = 250\,\mu m$; Black circle point: Diesel.

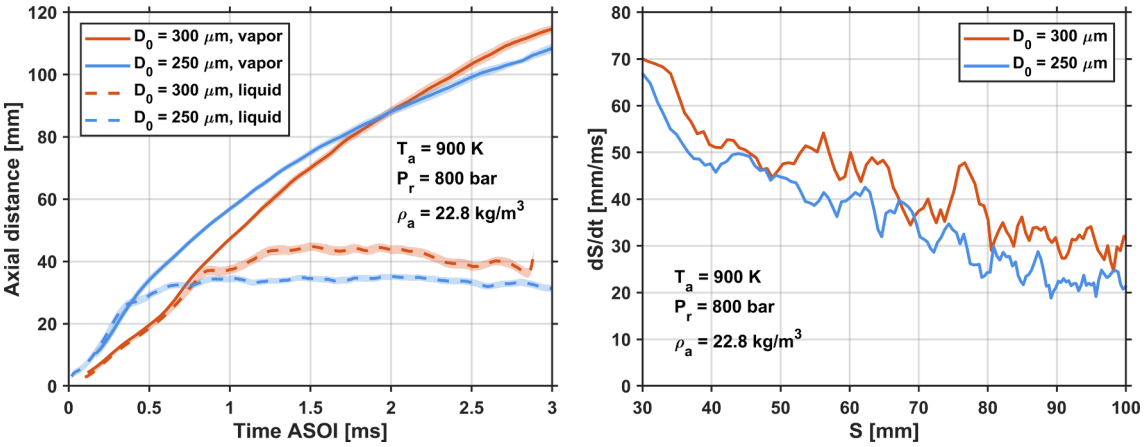

Fig. 10. Nozzle diameter effects on temporal liquid and vapor spray penetration (left) and spray tip propagation velocity dS/dt (right) for ammonia at the reference condition.

m^3, and the plots show results from the parametric variation together with different injection pressures for D300 (left) and D250 (right). It is noticeable that spray tip penetration is independent on the ambient temperature at constant air density, and a faster penetration was found at higher injection pressure due to the higher momentum (Eq. (2)). However, the performance along the time evolution shows differences. For D300, the acceleration to spray penetration at higher injection pressure was only significant downstream of 20 mm. For D250, the difference caused by the variation of injection pressure is only obvious downstream of 40 mm, where the spray is in fully vapor phase. Vapor spray penetration seems to be weakly dependent on ambient temperature, but this is closely related to the initial linear period, penetration rates during the quasi-steady phases are independent of ambient temperature.

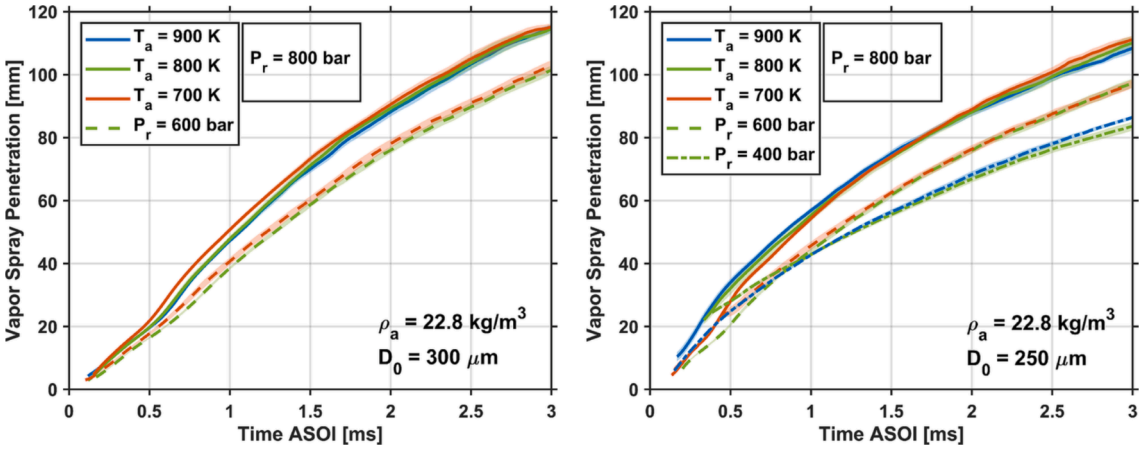

Fig. 11. Comparison of injection pressure and ambient temperature effects on vapor spray penetration for ammonia (left. $D_0 = 300\,\mu m$; right. $D_0 = 250\,\mu m$).

Finally, Fig. 12 presents the effect of ambient density on the penetration for D300 (left) and D250 (right) together with the variation of injection pressure. With an increase in ambient density, the higher air entrainment into the spray for a constant momentum flux results in a lower velocity and hence a decrease in penetration. However, the strong effect of the initial linear phase hides this evolution. Just as an example, for D300 a longer linear trend for the lower ambient density is obtained (roughly until 20 mm penetration). After that, the lower penetration rate with higher ambient density results in the expected shorter penetration after 60 mm. For D250, the discrepancy effect of ambient density is also visible since the start of injection, with a shorter linear period compared to D300. For the smaller nozzle, the well-known trend with a decreasing penetration with higher density can be found earlier due to the shorter linear period, and the effect is more significant at low injection pressure.

3.4. 1D model

To further investigate the mixing characteristics of inert ammonia spray, a 1D model developed by CMT was used to validate the liquid and vapor penetration and backup the observed trends. This model is based on mixing-controlled hypotheses it has been widely described in [39–41]. The spray was assumed to be injected into a quasi-steady environment, and the momentum exchange with the surrounding gas leads to the increase of spray radius as the spray propagation in axial direction. The computational domain is divided into a number of cells, and the on-axis velocity and fuel mass fraction of each cell are obtained by solving the conservation equations of momentum and fuel mass. The self-similar radial profile along the radial direction is assumed in the fully developed zone to allow for a 1D solution.

The main inputs to the model consist of thermodynamic conditions (shown in Table 2) and time evolution of injection (injection rate and momentum flux). Measuring rate of injection (ROI) for the liquid ammonia injection under the operating conditions was not possible. Instead, an 'educated' ROI used within the Engine Combustion Network (ECN) was employed here as a first approximation [42], which is available at CMT website [43]. To accommodate the injection rate to the present larger nozzles, the model ROI was scaled according to the corresponding diameters, and the slope of ramp up period was decreased consistently with an expected slower needle lift. Compared to cases where only a single spray cone angle is used, the approach discussed in [41,42] was followed, where spray angles for near- θ_1 and far-field θ_2 are used, with a transition occurring at an intact length distance IL from the orifice. The intact length was scaled with the nozzle diameter. A summary of the main input settings to the 1D model for Diesel and ammonia are at the standard condition is specified in Table 4.

A core topic for the 1D model is the calculation of state relationship to derive local conditions that can be used to solve the momentum and fuel conservation equations. When fuel injected into the chamber, the 1D model calculates local properties for both the liquid and gas phases. In the two-phase zone, the spray is assumed to be in liquid–vapor (LV) equilibrium under adiabatic saturation conditions. Fig. 13 presents the comparison of bubble and dew curves obtained from the LV equilibrium according to the methodology described in [41] and compared to experimental values in [44]. Ammonia properties are retrieved from NIST database [45] and its thermodynamic and transport properties are based on NASA 7-Coefficient Polynomial Parameterization [46]. For 10 MPa, which is lower than the critical pressure of ammonia (11.3 MPa), the maximum temperature occurs at pure fuel conditions, and it is equal to the corresponding saturation temperature (roughly 398 K). As the ambient pressure increases above ammonia critical pressure, the critical point shifts away from pure ammonia properties towards lower mass fractions, and the maximum temperature decreases.

Fig. 14 presents the temperature (left) and fuel mass fraction in liquid and vapor phase (right) according to the reference operating conditions, i.e., fuel is injected at 288 K into the ambient of nitrogen at temperature of 900 K and density of 22.8 kg/m3. N-Hexadecane has been used as reported in [40] as a surrogate fuel to Diesel in the simulation. Fuel stream conditions occur at the position f = 1, corresponding to a temperature at 288 K, while pure air is found at f = 0, T = 900 K. For both fuels, liquid phase only occurs near the vicinity of the injector. As the temperature of the mixture increases due to air entrainment, it transitions into the liquid–vapor equilibrium zone and eventually reaches the vapor phase zone at a given fevap value, concurrently with a monotonical decrease in mixture fraction.

The first important difference between both fuels is the higher volatility of ammonia, as denoted by the much lower dew and bubble temperature values. A second difference is the much lower increase in temperature of ammonia when moving towards lower mixture fraction, i.e., progressing from pure liquid to pure vapor states. This is a result of the high latent heat of vaporization. The fevap value is slightly lower for C16H34 (0.27) compared to ammonia (0.34), but there is a strong difference in the corresponding temperature (600 vs 330 K). This should have a strong effect on a potential start of chemical reactions, if this were

Table 4
The configurations of inputs to 1D model for Diesel and ammonia.

Item	Diesel	Ammonia
Spray angle, θ_1 [°]	15	13
Spray angle, θ_2 [°]	26	26
Intact length, IL [mm]	57	48/36
Nozzle diameter [μm]	300	300/250
Area coefficient Ca [–]	0.98	0.98
Discharge coefficient Cd [–]	0.8	0.8

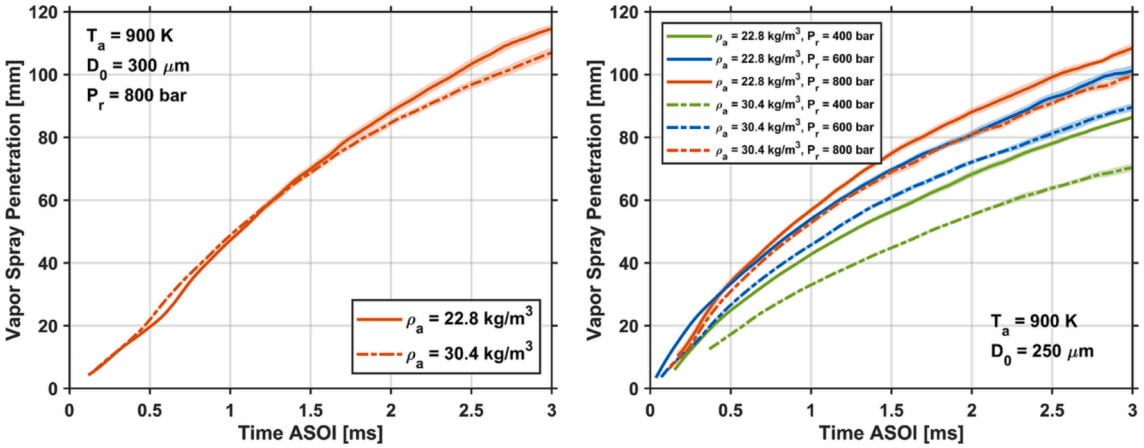

Fig. 12. Comparison of ambient density and injection pressure effects on vapor spray penetration for ammonia (left. D_0 = 300 μm; right. D_0 = 250 μm).

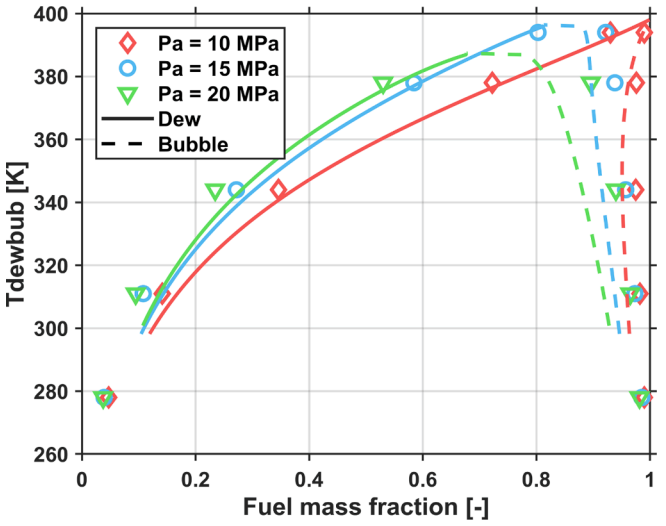

Fig. 13. Dew and bubble curves for nitrogen-ammonia at different ambient pressure.

a reacting case. Finally, the right plot shows that the evaporation of ammonia (increase in vapor mass fraction) occurs over a relatively wide mixture fraction range, while for C16H34 it only happens relatively close to the mixture fraction of evaporation.

The validation of 1D model on the liquid and vapor penetration is shown in Fig. 15. With the specifications in Table 4, a good prediction to the vapor penetration is achieved for Diesel using the penetration with the surrogate n-hexadecane fuel, but there is also deviation in the initial stage due to the simplified ramp up of stage at 'educated' ROI. Compared to Diesel, ammonia has a narrower spray and a shorter liquid length throughout DBI images, thereby, a smaller spray angle in the near field and a shorter intact length was considered for ammonia as the inputs for ammonia. As shown on the right figure, the calculated for ammonia also matches well with the experiment, but the vapor penetration is over-predicted (shown in 1D – S). Given the uncertainty in the injection rate availability for ammonia, it cannot be neglected that this could be due to the inability to correctly describe the initial transient needle lift. This can be demonstrated by the fact that just by shifting the start to injection in 1D model to 0.238 ms ASOI (1D – S, shift), then the calculated vapor penetration overlaps with the experiment. This indicates that current hypotheses of 1D model are still feasible on the calculation of the vapor phase, while the prediction to the initial phase needs to consider a more detailed analysis of the injector transient at the start of injection, where some effects probably due to the high volatility and large heat of vaporization of ammonia, as well as differences in viscosity have a strong effect on the effective injection rate. The detailed prediction of such effects is out of the present scope of activities.

Aside from the transient effects related to the tip penetration, the

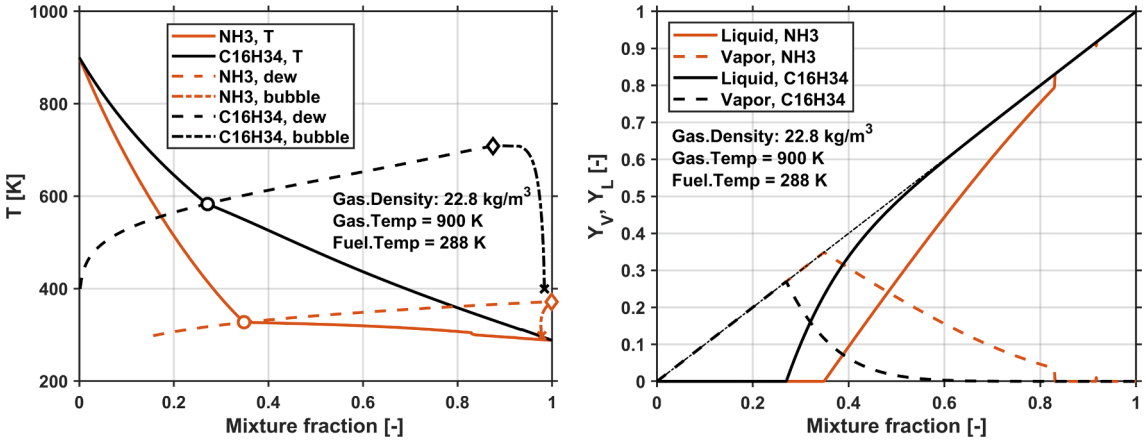

Fig. 14. Temperature evolution (left) and liquid and vapor fuel mass fraction (right) against the fuel mass fraction for liquid ammonia and Diesel at 288 K ejected into an ambient of nitrogen at density of 22.8 kg/m^3 and temperature of 900 K. Round marker: evaporation mixture fraction/temperature; diamond marker: critical point; cross marker: start of the evaporation mixture fraction.

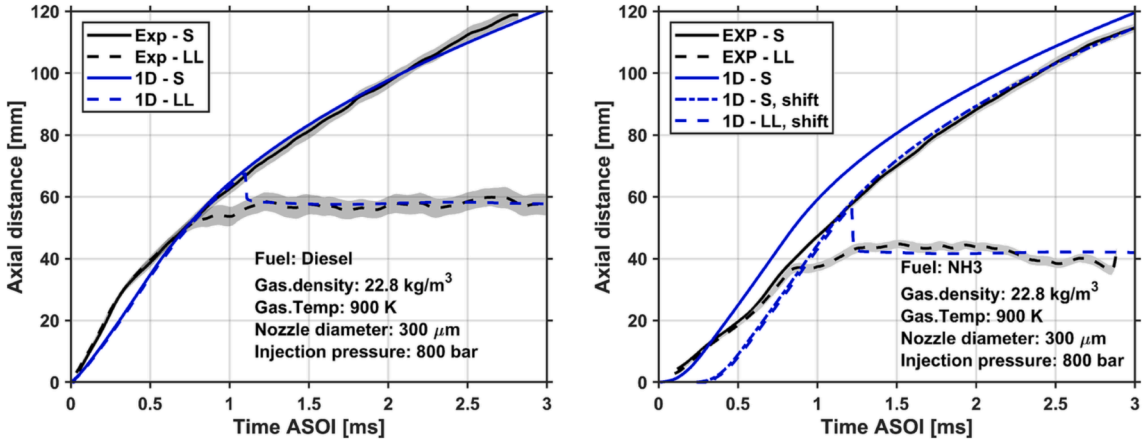

Fig. 15. The validation of 1D model on the vapor and liquid spray penetration for Diesel (left) and ammonia (right) at the standard condition (ρ_a = 22.8 kg/m^3, T_a = 900 K, D_0 = 300 μm, P_r = 800 bar).

quasi-steady maximum liquid length would not be affected by the transient initial ramp-up. Therefore, the 'educated' ROI is sufficient to validate the 1D model on liquid length for the conditions investigated. Fig. 16 presents the comparison of liquid length between the calculated results and the experimental data. Since the mixing-controlled vaporization was considered in 1D model, the predicted liquid length is fully consistent with description in Eq. (1). As suggested by Fig. 9 (right) the conditions where liquid length significantly deviates from the average are at the highest density of D300, and the lowest temperature of D250. This discrepancy is also observed in the comparisons here. Considering all points, it falls upon a straight line that goes through the origin with a slope of 1.0056 and a R-square value of 0.9951.

Overall, the previous results hint at the validity of the mixing-controlled approach for the analysis of ammonia sprays for the prediction of quasi-steady liquid length and fully-developed spray penetration. However, an accurate prediction of the initial tip penetration is still challenging in 1D model, and this is also the key problem in future analyses, e.g., by means of CFD simulations.

4. Conclusions

In this paper, the evolution of direct injection ammonia sprays under Diesel-like engine conditions has been investigated by means of diffused back-illumination imaging and single-pass schlieren techniques in a constant pressure facility. A single-orifice injector is used to enable accurate control of the flow through the orifice. The back pressure of the injector return-leakage line has been increased up to 10 bar, and the injector holder cooling fluid is brought down to a temperature of 15 °C. Both measures enable stable injector operating by preventing flashing conditions from occurring within the injector, in particular within the control volume. The experimental conditions include relevant operating parameters, such as injection pressure (400 bar to 800 bar), ambient temperature (700 K to 900 K), ambient density (22.8 kg/m3 and 30.4 kg/m3), and nozzle diameter (250 μm and 300 μm). Diesel is also used as a reference fuel. A well-stablished 1D spray model has been employed to analyse the mixing characteristics of the inert spray. From the analysis of the results, the observations can be summarized as follows:

)1. During the initial injection phase, a linear increment of penetration with time has been observed, with a later transition to a typical mixing-controlled penetration phase. Compared to Diesel, ammonia exhibits a slower propagation speed in the initial phase, and a similar propagation speed in the fully developed zone. The initial lag in start of injection for ammonia results in a shorter penetration for both liquid and vapor phases. A larger nozzle or a lower injection pressure causes slower ramp up in the needle lift, and a slower propagation in the initial phase.
)2. Similar to Diesel, liquid length with ammonia eventually reaches a quasi-steady value, which follows similar trends as those found in the literature for Diesel-like sprays. Liquid length is shorter with increasing ambient temperature and gas density and increasing nozzle diameter, and it is almost not affected by injection pressure. Derived experimental values can be normalized based upon mixing-control concepts within an uncertainty of 6.3 %.
)3. The similar spray profile in the vapor phase between Diesel and ammonia hints at a similar correlation of vapor penetration with ambient density, nozzle diameter, injection velocity and spray angle. A negligible effect is found with ambient temperature.
)4. The application of the 1D spray model has shown that reasonable predictions can be delivered for the most relevant spray metrics, namely tip penetration and quasi-steady liquid length. This confirms that, except of the initial transient injection period, the behaviour of high pressure direct-injection ammonia sprays follows most of the trends found in the literature for Diesel-like sprays. This is especially evident for the quasi-steady liquid length, which can be predicted based upon mixing-controlled arguments.
)5. Further efforts are needed to resolve the starting injection period and understand the behaviour of ammonia within the injector body that may result in the slow needle ramp up. Additionally, the quantification of the injection rate shapes is also a critical input for the quantification of spray evolution in any kind of predictive model.

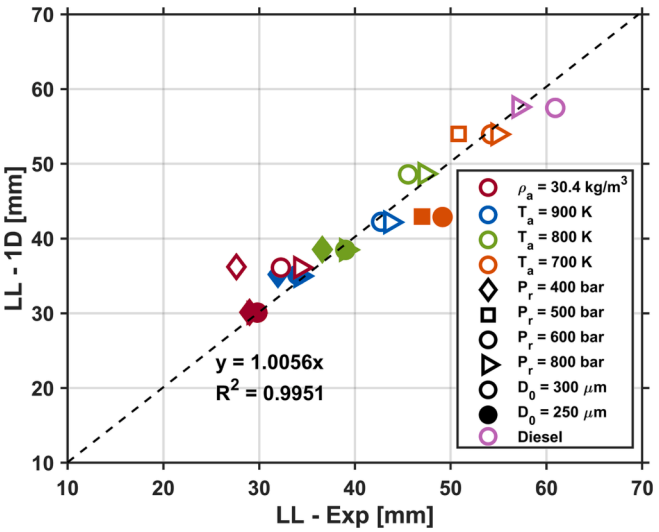

Fig. 16. Experimental and modelled liquid length for ammonia and Diesel. The ambient conditions are characterized by different colours, the difference on injection pressure is marked by different symbols. Solid and empty symbols are used for D250 and D300, respectively.

CRediT authorship contribution statement

Raul Payri: Project administration, Funding acquisition, Conceptualization. **José M. García-Oliver:** . **Gabriela Bracho:** Writing – original draft, Methodology, Investigation, Data curation, Conceptualization. **Jiawei Cao:** Writing – original draft, Methodology, Investigation, Data curation.

Declaration of competing interest

The authors declare that they have no known competing financial interests or personal relationships that could have appeared to influence the work reported in this paper.

Data availability

Data will be made available on request.

Acknowledgments

This research has been partially funded by MCIN/AEI/10.13039/501100011033 and the European Union"NextGenerationEU"/PRTR as part of the project DIGIAMMONIA TED2021-129379A-I00. We also acknowledge the finance support from Chinese Scholarship Council (No. 201808320236). We would like to thank José Enrique del Rey and Omar Huerta for their valuable support during the experimental campaign.

References

[1] Jeong SY, Jang D, Lee MC. Property-based quantitative risk assessment of hydrogen, ammonia, methane, and propane considering explosion, combustion, toxicity, and environmental impacts. J Storage Mater 2022;54.

[2] E. Comission. European Commission, EU Reference Scenario 2016, Tech. Rep.; 2016.
[3] Zhang Y, Xu L, Zhu Y, Xu S, Bai X. Numerical study on liquid ammonia direct injection spray characteristics under engine-relevant conditions. Appl Energy 2023;334:120680.
[4] Lewandowski M, Pasternak M, Haugsvær M, Løvas T. Simulations of ammonia spray evaporation, cooling, mixture formation and combustion in a direct injection compression ignition engine. Int J Hydrogen Energy 2023.
[5] Novella R, Pastor J, Gomez-Soriano J, Sánchez Bayona J. Challenges and directions of using ammonia as an alternative fuel for internal combustion engines. SAE Technical Paper 2023-01-0324, 2023.
[6] Valera-Medina A, Xiao H, Owen-Jones M, David W, Bowen P. Ammonia for power. Prog Energy Combust Sci 2018;69:63–102.
[7] Zaher M, Yousefi A, Dadsetan M, Liko B, Lafrance S, Guo H, et al. Characterization of soot emissions formed in a compression ignition engine cofired by ammonia and diesel. Fuel 2023;349.
[8] Scharl V, Sattelmayer T. Ignition and combustion characteristics of diesel piloted ammonia injections. Fuel Commun 2022;11.
[9] Westlye F, Ivarsson A, Schramm J. Experimental investigation of nitrogen based emissions from an ammonia fueled SI-engine. Fuel 2013;111:239–47.
[10] Mørch C, Bjerre A, Gøttrup M, Sorenson S, Schramm J. Ammonia/hydrogen mixtures in an SI-engine: engine performance and analysis of a proposed fuel system. Fuel 2011;90:854–64.
[11] Ryu K, Zacharakis-Jutz G, Kong S. Effects of gaseous ammonia direct injection on performance characteristics of a spark-ignition engine. Appl Energy 2014;116:206–15.
[12] Dimitriou P, Javaid R. A review of ammonia as a compression ignition engine fuel. Int J Hydrogen Energy 2020;11.
[13] Chiong M, Chong C, Ng J, Mashruk S, Chong W, Samiran N, et al. Advancements of combustion technologies in the ammonia-fuelled engines. Energ Conver Manage 2021;244.
[14] Bro K, Pedersen P. Alternative diesel engine fuels: an experimental investigation of methanol, ethanol, methane and ammonia in a D.I. diesel engine with pilot injection. SAE technical paper; 1977.
[15] Reiter A, Kong S. Demonstration of compression-ignition engine combustion using ammonia in reducing greenhouse gas emissions. Energy Fuels 2008;22(5):2963–71.
[16] Gross C, Kong S. Performance characteristics of a compression-ignition engine using direct-injection ammonia–DME mixtures. Fuel 2012;103:1069–79.
[17] Scharl V, Lackovic T, Sattelmayer T. Characterization of ammonia spray combustion and mixture formation under high-pressure, direct injection conditions. Fuel 2023;333.
[18] Frankl S, Gleis S, Karmann S, Prager M, Wachtmeister G. Investigation of ammonia and hydrogen as CO2-free fuels for heavy duty engines using a high pressure dual fuel combustion process. Int J Engine Res 2021;22:3196–208.
[19] Lu Z, Ye J, Gui Y, Lu T, Shi L, An Y, et al. Numerical study of the compression ignition of ammonia in a two-stroke marine engine by using HTCGR strategy. Energy 2023;276.
[20] Zhang Z, Li T, Chen R, Wang N, Wei Y, Dawei W. Injection characteristics and fuel-air mixing process of ammonia jets in a constant volume vessel. Fuel 2021;304:121408.
[21] Li T, Zhou X, Wang N, Wang X, Chen R, Li S, et al. A comparison between low- and high-pressure injection dual-fuel modes of diesel-pilot-ignition ammonia combustion engines. J Energy Inst 2022;102.
[22] Pastor JV, Garcia-Oliver JM, Mico C, Garcia-Carrero AA. An experimental study with renewable fuels using ECN Spray A and D nozzles. Int J Engine Res 2021:1748–59.
[23] Payri R, Gimeno J, Bardi M, Plazas AH. Study liquid length penetration results obtained with a direct acting piezo electric injector. Appl Energy 2013:152–62.
[24] Vera-Tudela Fajardo WM. Artist, An experimental study of the effects of fuel properties on diesel spray processes using blends of single-component fuels. [Art]. Polytechnic University of Valencia. Department of Thermal Machines and Motors - Department of Thermal Machines and Motors; 2015.
[25] T. E. ToolBox, "Ammonia - Thermophysical Properties," [Online]. Available: https://www.engineeringtoolbox.com/ammonia-d_1413.html. [Accessed 12 12 2023].
[26] Engine Conbustion Network, Liquid Penetration Length, [Online]. Available: https://ecn.sandia.gov/diesel-spray-combustion/experimental-diagnostics/liquid-penetration-length/. [Accessed 13 10 2023].
[27] Payri R, Viera JP, Gopalakrishnan V, Szymkowicz PG. The effect of nozzle geometry over the evaporative spray formation for three different fuels. Fuel 2017;188(15):645–60.
[28] Gimeno J, Bracho G, Marti-Aldaravi P, Peraza JE. Experimental study of the injection conditions influence over n-dodecane and diesel sprays with two ECN single-hole nozzles. Part I: Inert atmosphere. Energ Conver Manage 2016;126(15):1146–56.
[29] Settles G. Schlieren and Shadowgraph Techniques. Heidelberg: Springer, Berlin; 2001.
[30] Pastor JV, Payri R, Garcia-Oliver JM, Nerva J-G. Schlieren measurements of the ECN-spray a penetration under inert and reacting conditions. In: SAE 2012 World Congress & Exhibition; 2012.
[31] Siebers DL. Liquid-Phase Fuel Penetration in Diesel Sprays. In SAE Technical Paper 980809; 1998.
[32] Peraza JE, Salvador FJ, Gimeno J, Ruiz S. ECN Spray D visualization of the spray interaction with a transparent wall under engine-like conditions. Part I: Non-reactive impinging spray. Fuel 2022;307:121699.
[33] Espey C, Dec JE. The effect of TDC temperature and density on the liquid-phase fuel penetration in a D.I. diesel engine. In: SAE International Fall Fuels and Lubricants Meeting and Exhibition 952456, 1995.
[34] Zhou X, Li T, Wei Y, Wang N. Scaling liquid penetration in evaporating sprays for different size diesel engines. Int J Engine Res 2020;21(9):1662–77.
[35] Pickett LM, Manin J, Genzale CL, Siebers DL, Musculus MPB, Idicheria CA. Relationship between diesel fuel spray vapor penetration/dispersion and local fuel mixture fraction. In: SAE Technical Paper 2011-01-0686; 2011.
[36] Naber JD, Siebers DL. Effects of gas density and vaporization on penetration and dispersion of diesel sprays. In: SAE Technical Paper 960034; 1996.
[37] Desantes JM, Arregle J, Javier Lopez J, Cronhjort A. Scaling laws for free turbulent gas jet and diesel-like sprays. Atomization Sprays 2006;16(4):443–74.
[38] Desantes JM, Payri R, Salvador F, Gil A. Development and validation of a theoretical model for diesel spray penetration. Fuel 2006;85(7–8):910–7.
[39] Paster JV, Javier Lopez J, Garcia-Oliver JM, Pastor JM. A 1D model for the description of mixing-controlled inert diesel sprays. Fuel 2008;87(13–14):2871–85.
[40] Desantes JM, Pastor JV, Garcia-Oliver JM, Pastor JM. A 1D model for the description of mixing-controlled reacting diesel sprays. Combust Flame 2009;156(1):234–49.
[41] Pastor JV, Garcia-Oliver JM, Pastor JM, Vera-Tudela W. One-dimensional diesel spray modeling of multicomponent fuels. Atomization Sprays 2015;25(6):485.
[42] Pickett LM, Manin J, Payri R, Bardi M, Gimeno J. Transient rate of injection effects on spray development. In: SAE, 11th International Conference on Engines & Vehicles; 2013.
[43] CMT, Spray C/D Rate of injection, [Online]. Available: https://www.cmt.upv.es/#/ecn/download/nozzlecharac/ncSprayCDRateOfInj. [Accessed 23 10 2023].
[44] Reamer HH, Sage BH. Phase behaviour in the nitrogen-ammonia system. J Chem Eng Data 1959;4(4):303–5.
[45] L. P, NIST chemistry WebBook, NIST standard reference database 69, National Institute of Standards and Technology, [Online]. Available: https://webbook.nist.gov/cgi/cbook.cgi?Name=ammonia&Units=SI. [Accessed 23 10 2023].
[46] Mcbride BJ, Gordon S, Reno MA. Coefficients for calculating thermodynamic and transport properties of individual species. 6 9 2013. [Online]. Available: https://ntrs.nasa.gov/citations/19940013151. [Accessed 31 10 2023].
[47] Yu Z, Li X, Zhao J. Development of Ammonia Reaction Kinetic Mechanism under Engine-Relevant Conditions. Energy&Fuels 2024;(38):728–41.